J. Fluid Mech. (2014), *vol.* 752, *pp.* 22–38.
doi:10.1017/jfm.2014.319

Self-propelled jumping upon drop coalescence on Leidenfrost surfaces

Fangjie Liu[1], Giovanni Ghigliotti[2,‡], James J. Feng[2,3] and Chuan-Hua Chen[1,†]

[1]Department of Mechanical Engineering and Materials Science, Duke University, Durham, NC 27708, USA

[2]Department of Mathematics, University of British Columbia, Vancouver, BC, Canada V6T 1Z2

[3]Department of Chemical and Biological Engineering, University of British Columbia, Vancouver, BC, Canada V6T 1Z3

(Received 7 October 2013; revised 28 May 2014; accepted 31 May 2014)

Self-propelled jumping upon drop coalescence has been observed on a variety of textured superhydrophobic surfaces, where the jumping motion follows the capillary–inertial velocity scaling as long as the drop radius is above a threshold. In this paper, we report an experimental study of the self-propelled jumping on a Leidenfrost surface, where the heated substrate gives rise to a vapour layer on which liquid drops float. For the coalescence of identical water drops, we have tested initial drop radii ranging from 20 to 500 μm, where the lower bound is related to the spontaneous takeoff of individual drops and the upper bound to gravitational effects. Regardless of the approaching velocity prior to coalescence, the measured jumping velocity is around 0.2 when scaled by the capillary–inertial velocity. This constant non-dimensional velocity holds for the experimentally accessible range of drop radii, and we have found no cutoff radius for the scaling, in contrast to prior experiments on textured superhydrophobic surfaces. The Leidenfrost experiments quantitatively agree with our numerical simulations of drop coalescence on a flat surface with a contact angle of 180°, suggesting that the cutoff is likely to be due to drop–surface interactions unique to the textured superhydrophobic surfaces.

Key words: breakup/coalescence, condensation/evaporation, drops and bubbles

1. Introduction

Liquid drops merging on superhydrophobic surfaces (Quéré 2005) can spontaneously jump out of the plane upon coalescence (Boreyko & Chen 2009). The self-propelled motion has both biological relevance and engineering applications as reviewed in our companion paper (Liu *et al.* 2014). Since the kinetic energy of the jumping ($\sim\rho_L r_0^3 \bar{v}_j^2$)

† Email address for correspondence: chuanhua.chen@duke.edu

‡ Present address: Laboratoire de Physique de la Matière Condensée, CNRS UMR 7336, Université de Nice Sophia-Antipolis, Parc Valrose, 06108 Nice CEDEX 2, France.

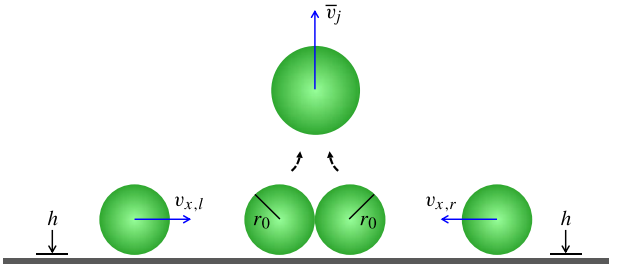

FIGURE 1. (Colour online) Schematic of the coalescence-induced jumping on a Leidenfrost substrate: two identical drops with an initial radius r_0 coalesce into a larger drop with an equilibrium radius of $r = 2^{1/3} r_0$. The reduction in surface area releases excess surface energy, powering the merged drop to jump away from the substrate with a vertical jumping velocity $\bar{v}_j$. On the heated substrate, the drops float on a vapour layer of thickness h, and approach each other with a relative velocity of $v_{app} = |v_{x,l} - v_{x,r}|$.

is converted from the surface energy released upon drop coalescence ($\sim \sigma r_0^2$), the mass-averaged jumping velocity ($\bar{v}_j$) follows the capillary–inertial scaling (u_{ci}),

$$\bar{v}_j \sim u_{ci} = \sqrt{\frac{\sigma}{\rho_L r_0}}, \tag{1.1}$$

where σ is the surface tension, ρ_L is the liquid density and r_0 is the radius of two identical drops prior to coalescence; see Liu *et al.* (2014) for more details. In our initial report (Boreyko & Chen 2009), the self-propelled motion resulting from a symmetric coalescence is perpendicular to the substrate and the jumping velocity indeed follows the capillary–inertial scaling. However, there exists a cutoff radius of approximately 30 μm, below which the capillary–inertial scaling no longer applies (Boreyko & Chen 2009).

In our companion paper, we present a simplified numerical model to investigate the jumping mechanism (Liu *et al.* 2014). Although our numerical simulations faithfully capture the self-propelled process and the associated jumping velocity, the predicted cutoff radius (due to viscous effects) for the capillary–inertial scaling is two orders of magnitude smaller than that reported on superhydrophobic surfaces. In the model, two initially static drops with identical radii coalesce on a flat non-wetting substrate with a contact angle of 180°. Such a boundary condition neglects the drop–surface adhesion as well as the dynamic interaction between the coalescing drops and the textured superhydrophobic surface. The primary purpose of this paper is to experimentally validate the numerical model by studying the self-propelled jumping on Leidenfrost surfaces (Leidenfrost 1756; Gottfried, Lee & Bell 1966; Bernardin & Mudawar 1999; Quéré 2013), which presumably approximate the simplified non-wetting boundary condition better than textured superhydrophobic surfaces.

On a solid surface heated to a temperature above the Leidenfrost point (figure 1), a liquid drop floats above a vapour layer with an effective contact angle of 180° (Quéré 2013). The thin vapour layer separates the liquid drop from the surface and prevents violent boiling. The Leidenfrost drop is essentially at the boiling point of the working fluid, e.g. 100 °C for water under atmospheric pressure (Gottfried *et al.* 1966; Biance, Clanet & Quéré 2003; Burton *et al.* 2012). The Leidenfrost drop exhibits a nearly spherical shape resembling that of a superhydrophobic drop, with an important

distinction that the Leidenfrost drop is not in physical contact with the solid surface. As such, the flat Leidenfrost surfaces eliminate drop–surface adhesion as well as the complexity associated with moving contact lines, better approximating the conditions in the numerical model of Liu *et al.* (2014) as long as the vapour layer acts as a passive medium.

The Leidenfrost phenomenon hinges on the vapour layer separating the liquid drop and the solid surface. The vapour layer is thicker under the centre of the drop and thinner near the edge of the drop (Snoeijer, Brunet & Eggers 2009; Burton *et al.* 2012), and the average thickness varies strongly with the drop radius (Gottfried *et al.* 1966; Biance *et al.* 2003; Celestini, Frisch & Pomeau 2012). For relatively large drops, the average thickness of the vapour layer is governed by the balance between the weight of the liquid drop and the lubrication pressure of the vapour layer. As a result, the thickness increases with the drop radius (Gottfried *et al.* 1966; Biance *et al.* 2003). However, the well-known lubrication regime breaks down below a critical drop radius (r_{lub}) that scales as (Celestini *et al.* 2012; Pomeau *et al.* 2012)

$$r_{lub} = \left(\frac{\mu_V k_V \Delta T}{\rho_L \rho_V \lambda_{LV} g} \right)^{1/3}, \tag{1.2}$$

where μ_V, k_V and ρ_V are respectively the vapour viscosity, thermal conductivity and density, λ_{LV} is the latent heat of vaporization, ΔT is the temperature difference between the heated substrate and the liquid drop, and g is the gravitational acceleration. Below this critical radius, an individual Leidenfrost drop spontaneously takes off from the heated substrate, until the drop is much farther away with a lower evaporation rate. In the new regime, the weight of the drop is balanced by the drag of the upward vapour flow rather than the lubrication pressure (Celestini *et al.* 2012). Unlike larger Leidenfrost drops, for which the vapour layer thickness decreases with decreasing drop radius (Biance *et al.* 2003), smaller drops ($r_0 \lesssim r_{lub}$) exhibit increasing thickness with decreasing drop radius (Celestini *et al.* 2012).

Building upon the work of Boreyko & Chen (2010), we report below the coalescence-induced jumping phenomenon on Leidenfrost surfaces. Using high-speed video imaging, the self-propelled processes are captured and the jumping velocities measured over a wide range of drop radii. To test the numerical model in our companion paper (Liu *et al.* 2014), particular attention will be paid to the verification of the capillary–inertial scaling law in (1.1) as well as any potential deviation indicating a cutoff.

2. Experimental methods

The self-propelled jumping of deionized water drops is studied on a Leidenfrost surface schematically shown in figure 2. For initial drop radii from 20 to 500 μm, the range accessible by our set-up, the jumping velocities are extracted from the trajectories of the merged drop.

2.1. *Experimental set-up*

Under atmospheric conditions, the aluminium stage in figure 2 is heated above the Leidenfrost point for water drops to float on a vapour layer. Two cartridge heaters (Omega CIR-1021) are inserted beneath the Leidenfrost surface and powered through a temperature controller (Omega CNi3243). The temperature of the Leidenfrost surface where coalescence occurs is measured by a K-type thermocouple inserted

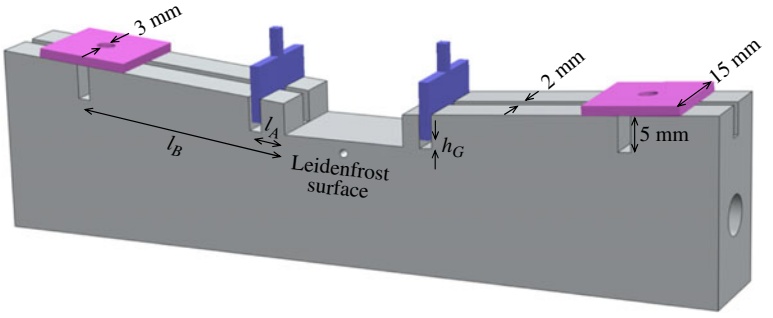

FIGURE 2. (Colour online) Schematic of the experimental set-up for drop coalescence on a heated Leidenfrost stage. The schematic is drawn to scale, with a few omissions of non-essential details. The aluminium stage is heated by two cartridge heaters inserted from the sides, and its temperature is monitored by a thermocouple inserted 2 mm underneath the centre of the Leidenfrost surface. Water drops are guided by 2 mm wide grooved ramp(s) slanted at an angle of 5° towards the flat centre surface with a dimension of 20 mm × 15 mm. Two gate positions are used, corresponding to ramp lengths of $l_A =$ 5 mm and $l_B = 40$ mm, respectively. As detailed in the text, three operating modes are used depending on the drop radii of interest.

2 mm underneath the surface. The Leidenfrost surface is heated to be at $250 \pm 1\,^{\circ}\mathrm{C}$, significantly higher than the measured Leidenfrost point of 195 °C for deionized water drops. Note that both temperatures are measured by an inserted thermocouple, so the temperatures of the actual Leidenfrost surface should be somewhat lower. The coalescence process is recorded by a high-speed camera (Phantom V7.1 or V710) attached to a long-distance microscope (Infinity K2). Typical frame rates are 800 or 1000 frames per second (f.p.s.), but higher frame rates of up to 6000 f.p.s. are also used to capture the detailed jumping process. The exposure time is kept below 10 % of the frame interval to prevent motion blur.

In the Leidenfrost experiments, the drop radii immediately before and after coalescence can be assumed to be unaffected by the phase-change process. This is a good assumption because the phase-change process is much slower than the jumping process, which is governed by the capillary–inertial time scale (Boreyko & Chen 2009; Liu *et al.* 2014),

$$\tau_{ci} = \sqrt{\frac{\rho_L r_0^3}{\sigma}}. \tag{2.1}$$

As an example, the evaporating Leidenfrost drops in our experiments have a typical life span well over 10 s (Quéré 2013), whereas the jumping process often takes place well within 10 ms according to (2.1), as experimentally confirmed below.

Our Leidenfrost set-up in figure 2 offers a few advantages in studying the self-propelled jumping phenomenon when compared to the often-adopted set-up using coalescence of growing condensate drops on superhydrophobic surfaces (Boreyko & Chen 2009). (i) Flat Leidenfrost surfaces are much more robust than microtextured superhydrophobic surfaces, enabling exquisite controls such as gated release of coalescing drops of predetermined radii. (ii) The coalescence process of two Leidenfrost drops can be visualized without the optical blockage of neighbouring condensate drops on the substrate, enabling detailed study of the drop–surface interaction during the entire jumping process. (iii) As discussed earlier, the boundary

condition on Leidenfrost surfaces is simpler than that on superhydrophobic surfaces as long as the vapour layer acts as a passive medium, permitting validation of our numerical model in Liu *et al.* (2014) from a different angle. (iv) Although not exploited in this paper, the Leidenfrost set-up permits the study of additional liquids such as ethanol (Boreyko 2012), for which a superlyophobic surface is difficult to construct particularly in a condensing environment.

2.2. *Variation of drop radii*

The jumping velocities are measured for initial drop radii from 20 to 500 μm, the range accessible by our Leidenfrost set-up in figure 2. The lower bound of the experimentally accessible radii is related to the critical radius in (1.2) for the spontaneous takeoff of individual Leidenfrost drops (Celestini *et al.* 2012), which is $r_{lub} = 15$ μm with the physical properties at 100 °C and a temperature difference of 150 °C as in our set-up. The upper bound is related to the capillary length, which is $\sqrt{\sigma/\rho_L g} = 2.5$ mm for water at 100 °C. The initial radius in our study is kept below 500 μm so as to neglect gravitational effects on the coalescence process. To change the drop radii over more than one order of magnitude, three variations of the experimental set-up are adopted depending on the desired radii.

For $r_0 \gtrsim 300$ μm, a colliding mode is used. Water drops of a desired volume are pipetted behind two initially closed gates ($h_G = 0$ in figure 2), which are lifted up by solenoid actuators (Pontiac Coil L-04PL012D-C) to simultaneously release the drops. To achieve smaller radii, the deposited drops are sometimes allowed to evaporate for a period of time prior to the gated release. To vary the approaching velocity, both gates are positioned with a ramp length of either $l_A = 5$ mm or $l_B = 40$ mm. This is the only mode where the grooves on both sides of the stage are used.

For 100 μm $\lesssim r_0 \lesssim$ 300 μm, an exploding mode is used. Without any gate, an aluminium plate with a 1.5 mm radius hole is placed on top of the grooved track with a ramp length of $l_B = 40$ mm. Since the plate is far away from the heated surface, its temperature is below the Leidenfrost point but above the boiling point of water. A drop with a diameter larger than the hole is deposited onto the hole. Because of boiling, the large drop explodes into smaller droplets, which in turn pass through the hole and slide down the tracks towards the horizontal centre stage. Since many tiny droplets are produced, particularly when a syringe is used to supply a stream of large drops, only one grooved track is needed for drop coalescence to be captured.

For $r_0 \lesssim 100$ μm, a gating mode is used with a ramp length of $l_A = 5$ mm. A small gap is maintained between the aluminium gate and the bottom surface of the grooved track. Since the gap inhibits effective heating, the gate is below the Leidenfrost point and a drop deposited behind the gate again experiences explosion because of boiling. Among the droplets generated, only those with diameters smaller than the gap height (h_G) can pass through to reach the Leidenfrost surface in the centre. Depending on the desired drop radii, h_G is between 20 and 200 μm.

The desired colliding mode unfortunately cannot be used for drops below 300 μm, which tend to be bouncy and are also difficult to align for head-on collision with the 2 mm wide grooves. Smaller drops are studied with the exploding and gating modes, for which only one side of the stage is used. Care is taken to exclude data when strong vapour flow associated with the boiling explosion is detected above the Leidenfrost surface. In these two modes, the timing and location of the coalescence among exploded droplets are unpredictable. We therefore use relatively low video frame rates that are still adequate for measuring the jumping velocity, the main subject of interest.

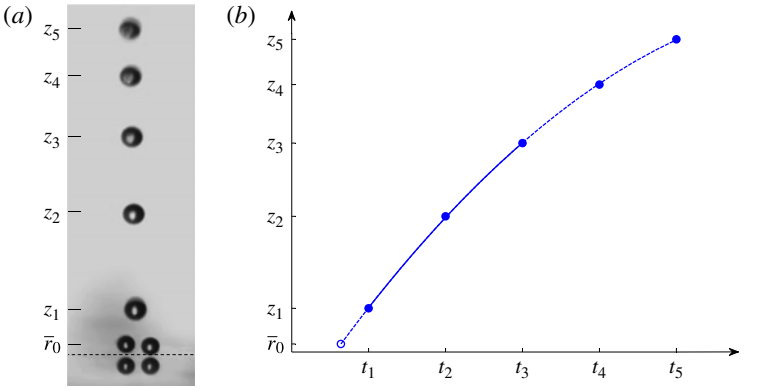

FIGURE 3. (Colour online) Trajectory of the merged drop used to extract the jumping velocity for an average initial radius of $\bar{r}_0 = 22$ μm. (*a*) The jumping process is illustrated by overlaid images taken at a time interval of 1.25 ms. Note that the coalescing drop on the left is slightly out of focus, approaching the other drop from behind. (*b*) The jumping velocity of $\bar{v}_j = 0.23$ m s^{-1} is extracted from a second-order polynomial fit (solid line) to the first three centre-of-mass locations (solid symbols), z_1, z_2 and z_3, recorded at a fixed time interval (δt) after the launching. The vertical locations are measured with respect to the Leidenfrost surface, whose position is fixed by the mirror image of an in-focus coalescing drop with its centre at $z = \bar{r}_0$ (open symbol). See also supplementary movie 1 available at http://dx.doi.org/10.1017/jfm.2014.319.

2.3. *Extraction of jumping velocities*

The jumping velocity ($\bar{v}_j$) is measured from drop trajectories for a wide range of average initial radius ($\bar{r}_0$). The trajectory of the merged drop is recorded using the 'centre of mass' based on two-dimensional video images. To accurately extract the departure velocity from the trajectory of the merged drop, the decelerations due to gravity and/or viscous drag should be accounted for. A representative jumping process is shown in figure 3(*a*), which overlays the time-lapsed images. After departure from the Leidenfrost surface, the merged drop decelerates as a consequence of air friction in addition to gravity. In figure 3(*b*), the vertical trajectory of the merged drop is well fitted by a second-order polynomial, indicating an approximately constant deceleration. The jumping velocity is extracted from the second-order polynomial fit constructed from the first three locations of the merged drop after its departure, $\tilde{z} = \tilde{z}(z_1, z_2, z_3, \delta t)$, where δt is the inter-frame interval of the video imaging. The jumping velocity ($\bar{v}_j$) is extracted as $(\mathrm{d}\tilde{z}/\mathrm{d}t)|_{z_1}$, the derivative of the polynomial fit evaluated at the first captured location after the drop has departed the surface. The lower bound of the velocity is given by $(z_2 - z_1)/\delta t$ which is solely based on experimental measurements. The upper bound is given by $(\mathrm{d}\tilde{z}/\mathrm{d}t)|_{\bar{r}_0}$ which is the derivative of the polynomial fit evaluated at $z = \bar{r}_0$, approximately the lowest possible centre of mass for a departing merged drop (e.g. $t = 2.67$ ms in figure 4).

The polynomial fit outlined above is used for all measurements of jumping velocities. Although more data points are available in many cases, the three-point polynomial fits are found to be consistent with extractions from more points; see for example figure 3(*b*). The validity of this second-order fit can be understood from two representative cases, the small drops with $\bar{r}_0 = 22$ μm in figure 3 and the large drops with $\bar{r}_0 = 380$ μm in figure 4, which essentially encompass the entire range of measurements from 20 to 500 μm.

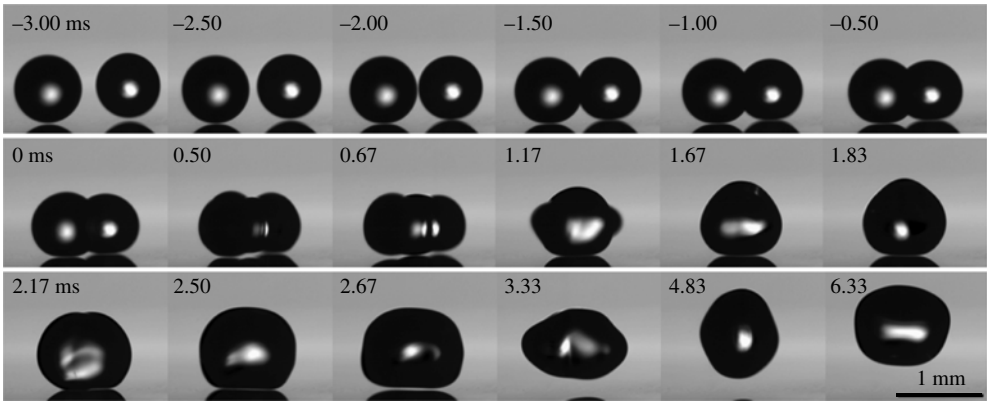

FIGURE 4. Self-propelled jumping process on a Leidenfrost surface upon coalescence of drops with an average initial radius of $\bar{r}_0 = 380$ μm. The left drop with a radius of 390 μm moves at $v_{x,l} = 0.07$ m s^{-1} and the right drop with a radius of 370 μm moves at $v_{x,r} = -0.09$ m s^{-1}, both measured with respect to the laboratory frame when the drops are about one diameter apart. At a relative velocity of $v_{app} = 0.16$ m s^{-1}, the two drops approach each other at an angle of approximately 45° from the optical axis. At 0 ms, a liquid bridge forms between the drops and the expanding bridge eventually impinges upon the bottom substrate (around 0.83 ms). The interaction between the merged drop and the substrate leads to the upward jumping at $\bar{v}_j = 0.08$ m s^{-1}, with the merged drop departing the surface between 2.5 and 2.67 ms. See also supplementary movie 2.

For the low-Reynolds-number motion of a merged drop moving in the air as in figure 3(*a*), the friction on the liquid drop is dominated by the Stokes drag. With a merged drop of radius $r = 2^{1/3} r_0$ at an initial jumping velocity $\bar{v}_j$, the Reynolds number for the motion in the air is $Re_G = \rho_{G0} \bar{v}_j r / \mu_G$, where ρ_{G0} is the air density (with the subscript 0 used for consistency with Liu *et al.* (2014)) and μ_G is the air viscosity. Neglecting gravity and the inertia of the surrounding air, the decelerating trajectory adopts the form

$$z = \bar{v}_j \tau_v (1 - \mathrm{e}^{-t/\tau_v}) = \bar{v}_j \tau_v \left(\frac{t}{\tau_v} - \frac{1}{2} \frac{t^2}{\tau_v^2} + \frac{1}{6} \frac{t^3}{\tau_v^3} + \cdots \right) \approx \bar{v}_j t - \tfrac{1}{2} \bar{a}_v t^2, \tag{2.2}$$

where the viscous time constant is $\tau_v = (2/9) \rho_L r^2 / \mu_G$. At early times, the trajectory in (2.2) can be approximated by a second-order polynomial with a nearly constant deceleration rate of $\bar{a}_v = \bar{v}_j / \tau_v$, which strictly speaking is the deceleration at the initial launching. Based on the Taylor expansion, the second-order approximation is accurate to within 2 % for $t \leqslant \tau_v / 2$. With $\bar{r}_0 = 22$ μm ($r = 28$ μm) and $\bar{v}_j = 0.23$ m s^{-1} in figure 3, $Re_G = 0.27$, justifying the low-Reynolds-number assumption. The viscous time constant is $\tau_v = 7.5$ ms and the viscous deceleration rate is $\bar{a}_v = 31$ m s^{-2}, justifying the neglect of gravity compared to viscous drag as a first approximation.

For a much larger drop with the deceleration dominated by gravity as in figure 4, the trajectory is still described by a second-order polynomial,

$$z = \bar{v}_j t - \tfrac{1}{2} g t^2. \tag{2.3}$$

With $\bar{r}_0 = 380$ μm ($r = 480$ μm) and $\bar{v}_j = 0.08$ m s^{-1} in figure 4, $Re_G = 1.6$, so it is still reasonable to use the Stokes drag as a first approximation to the air drag. The corresponding viscous time constant is $\tau_v = 2.2$ s and the viscous deceleration rate is $\bar{a}_v = 0.04$ m s^{-2}, justifying the dominance of gravity for the deceleration.

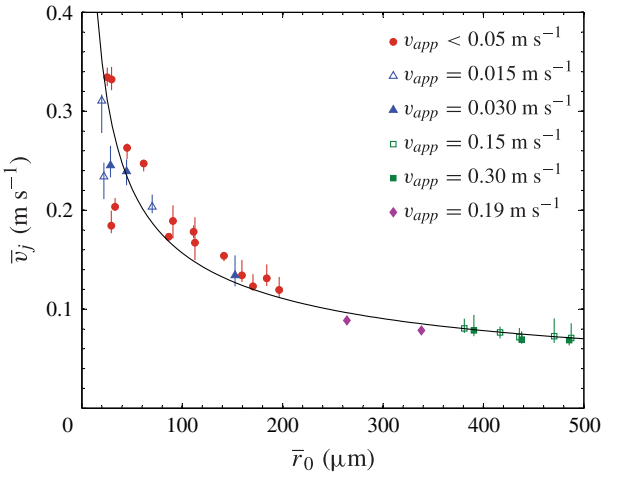

FIGURE 5. (Colour online) The jumping velocity ($\bar{v}_j$) upon drop coalescence is measured for a range of average initial radii ($\bar{r}_0$), where the radius disparity of two coalescing drops is kept within 15 %. The jumping velocity is independent of the relative approaching velocity (v_{app}), which is orthogonal to the jumping direction and is measured when the two drops are at least one diameter apart. The coalescence is roughly symmetric and the resulting jumping velocity is predominantly vertical, except for two data points around $\bar{r}_0 \approx 300$ μm. Therefore, only the vertical component is reported for the jumping velocity. The error bars are based on the confidence in the velocity extraction from a second-order polynomial fit of the drop trajectory. The solid line represents a power-law fit with $\bar{v}_j = 0.2u_{ci} \sim \bar{r}_0^{-1/2}$.

2.4. *Jumping velocities upon low-Weber-number coalescence*

With our experimental set-up, there is always some approaching velocity that reflects the horizontal motion of one or both of the Leidenfrost drops prior to coalescence (figure 1). However, the measured jumping velocity is insensitive to the approaching velocity in the low-Weber-number regime (figure 5). The Weber number represents the relative importance of inertia to capillarity,

$$We = \frac{\rho v^2 r_0}{\sigma}, \tag{2.4}$$

where v is a characteristic velocity. The low-Weber-number regime is ensured by restricting the relative approaching velocity of the two coalescing drops to be smaller than the capillary–inertial velocity ($v_{app} < u_{ci}$), such that $We < 1$. Note that two approaching drops do not necessarily coalesce (Neitzel & Dell'Aversana 2002), an example being the non-coalescing collision between a water drop and an ethanol drop on a Leidenfrost surface (Boreyko 2012). However, as long as the two drops are both made of water and the coalescence is in the low-Weber-number regime, similar to the 'regime I' coalescence in Qian & Law (1997), approaching drops are observed always to merge into one.

In the colliding mode with large drops, the approaching velocity is usually higher than the jumping velocity but still satisfies $v_{app} < u_{ci}$. The gate locations are the same on both sides to ensure an approximately symmetric coalescence. When the colliding drops are simultaneously released from both sides, the approaching velocity produced

by the longer ramp (l_B in figure 2) is roughly twice that produced by the shorter one (l_A). However, the jumping velocity in figure 5 is unchanged within experimental uncertainty.

The exploding and gating modes rely on drop explosion upon boiling to generate smaller droplets. In these two modes, the experiments are repeated over long periods of time to obtain desirable cases of low-Weber-number drop coalescence according to two criteria. First, the coalescing drops have approximately equal radii with a maximum difference of 15 %, and the roughly symmetric coalescence produces a predominantly vertical jumping. (For asymmetric coalescence with larger disparities in drop radii, see appendix A.) Second, the coalescing drops happen to be 'settled' on the Leidenfrost surface, with the drop–surface gap comparable to the vapour layer thickness of corresponding static drops. With these restrictions, the measured jumping velocity is again not sensitive to the approaching velocity (figure 5).

3. Results and discussions

The Leidenfrost experiments are now compared with the numerical simulations detailed in our companion paper (Liu *et al.* 2014). In the numerical model, two initially static drops with identical radii coalesce on a flat non-wetting substrate with a contact angle of 180°. The model neglects the vapour layer between the Leidenfrost drops and the heated substrate, as well as any active vaporization from the drops. To model the Leidenfrost coalescence, the properties of both liquid and air are taken at 1 atm and 100 °C except for the air density. The numerical air density is approximately 20 times the physical value (ρ_{G0}), but this discrepancy is verified to be inconsequential as far as the jumping motion is concerned. In addition, gravity is neglected in the model since the drop radii investigated here are significantly smaller than the capillary length.

3.1. *Self-propelled jumping processes*

A representative jumping process obtained by the colliding mode is shown in figure 4. As noted earlier by Boreyko & Chen (2009, 2010), the liquid bridge connecting the two drops quickly expands to impinge upon the substrate; the interception by the substrate leads to lateral deformation and then perpendicular recoil of the merged drop, ultimately giving rise to the out-of-plane jumping motion. In figure 4, the drop on the right approaches the left drop from behind, and the line connecting the centres of mass is at an angle of approximately 45° from the imaging plane. In fact, most of the coalescence cases captured using the set-up in figure 2 are not completely in the imaging plane. Fortunately, such a misalignment in the horizontal plane does not affect the measurement of the vertical jumping velocity, which is the dominant component for nearly symmetric coalescence studied here. Although the estimate of the approaching velocity (v_{app}) is somewhat affected by the misalignment, the jumping velocity is insensitive to the approaching speed within the low-Weber-number coalescence regime, as shown in figure 5.

The numerical results corresponding to the jumping process in figure 4 are shown in figure 6 with the same average initial radius ($\bar{r}_0$). With corresponding time stamps in both figures, the simulation faithfully captures the topological change prior to the jumping departure as well as the motion of the departed drop. The simulation captures the average jumping velocity very well, with the numerical value of 0.076 m s^{-1} close to the experimental one of 0.08 m s^{-1}. Note that there is an uncertainty in the experimental point of coalescence due to the limited frame rate of the video imaging.

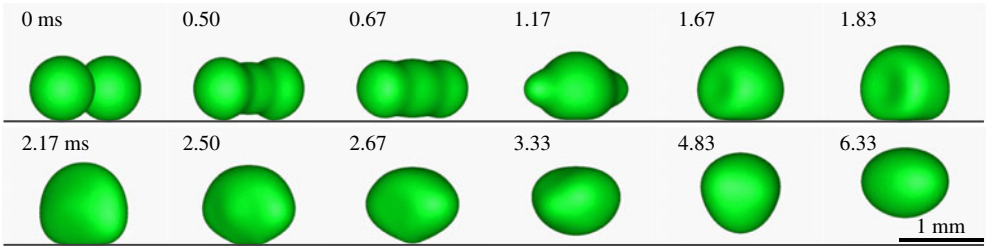

FIGURE 6. (Colour online) Simulated jumping motion upon drop coalescence on a non-wetting surface with a contact angle of 180°. To simulate the experimental results in figure 4, the initial drop radii are both set at $\bar{r}_0 = 380$ μm ($\tau_{ci} = 0.94$ ms), and the view angle is rotated 45°. The time stamps match those at the bottom two rows of figure 4. The numerical jumping velocity of $\bar{v}_j = 0.076$ m s^{-1} is extracted at 3.28 ms following procedures outlined in Liu *et al.* (2014). See also supplementary movie 3.

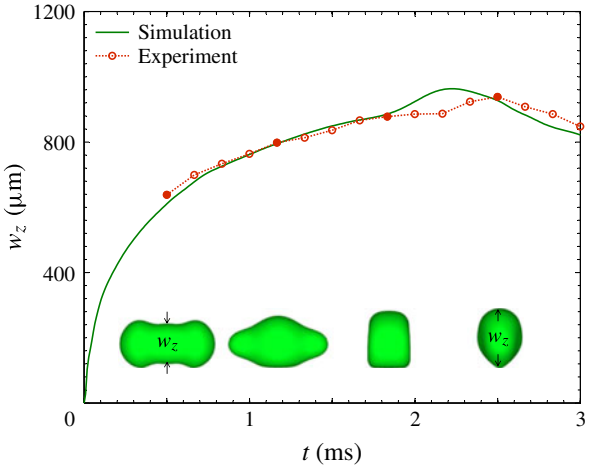

FIGURE 7. (Colour online) Measured and simulated evolution of the axial height (w_z) of the merged drop defined in the inset. The experimental $w_z(t)$ curve agrees well with the simulation from 0.5 to 1.83 ms, with 0.5 ms being the first trustworthy measurement because of the rotated view. The two curves intersect again at 2.5 ms, which is close to the point of departure. The four inset images are computed xz views of the merged drop at 0.5, 1.17, 1.83 and 2.5 ms, and these time stamps are also denoted by filled circles.

Since the coalescence is actually initiated between 0 and 0.17 ms in the experimental figure 4, the experimental drop profile at 1.83 ms should be compared with numerical profiles between 1.67 and 1.83 ms in figure 6. Unfortunately, the uncertainty in the exact angle of view precludes the pinpointing of the actual point of coalescence.

A more quantitative comparison of the topological change is shown in figure 7. Since the jumping motion originates from the impingement of the expanding liquid bridge, the numerical and experimental evolutions of the vertical bridge height (w_z) are compared. With a rotated view, the bridge height cannot be accurately assessed immediately after coalescence, so the first data point is taken at 0.5 ms. The bridge heights agree with each other till 1.83 ms, close to the first pseudo-equilibrium position, after which the merged drop starts to retract from the substrate (Liu *et al.*

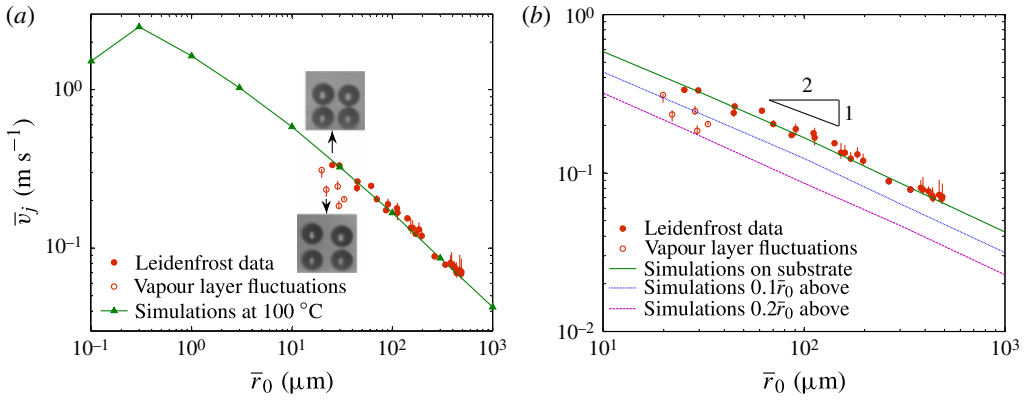

FIGURE 8. (Colour online) Comparison of the jumping velocities from experimental measurements and numerical simulations. (*a*) Both experiments and simulations follow the capillary–inertial scaling with the $\bar{v}_j \sim r_0^{-1/2}$ power law (parallel to the diagonal line). The numerical results exhibit a viscous cutoff radius of around 0.1 μm, which is not experimentally accessible because of significant fluctuations in the vapour layer thickness below 30 μm or so (open symbols). The fluctuations are evident by comparing inset images (132 μm × 132 μm) for $\bar{r}_0 = 25$ μm (top) and $\bar{r}_0 = 22$ μm (bottom), respectively. (*b*) The measurements are compared against simulations with a gap between the substrate and the bottom of the coalescing drops. The simulations are conducted at an initial radius of 10, 30, 100, 300 and 1000 μm. The numerical results with a gap of $0.1\bar{r}_0$ or $0.2\bar{r}_0$ seem to each follow the capillary–inertial scaling trend with a reduced prefactor. The open symbols associated with vapour layer fluctuations fall within the simulated trends without any gap (top solid line) and with a gap of $0.2\bar{r}_0$ (bottom dashed line).

2014). The discrepancy for the next period up to the moment of departure (between 2.5 and 2.67 ms) is likely to be related to the asymmetry in the coalescence process and the numerical approximation of the Leidenfrost surface by a passive non-wetting surface. The effect of the boundary condition is expected to be prominent close to the jumping departure, which results from the counter-action of the vapour layer on the substrate to the liquid bridge impingement. See further discussions in § 3.4.

3.2. *Capillary–inertial scaling*

In figure 8(*a*), the measured jumping velocities are compared with the numerical ones. The numerical results roughly follow the capillary–inertial scaling with $\bar{v}_j \sim r_0^{-1/2}$, as long as the initial radius is above the cutoff radius of 0.1 μm. The experimental data also follow the capillary–inertial scaling for the experimentally accessible range of radii down to approximately 20 μm, where the vapour layer thickness spontaneously fluctuates, as discussed below. Excluding these few data points with vapour layer fluctuations, the measured jumping velocities consistently follow the numerical results, with the experimental values being slightly higher (figure 8*b*). This subtle but consistent difference is probably a result of the dynamic role played by the vapour layer; see further discussions in § 3.4. The non-dimensional jumping velocity is approximately $\bar{v}_j^* \approx 0.2$ ($\bar{v}_j \approx 0.2u_{ci}$), and the corresponding conversion efficiency from the released surface energy to translational kinetic energy is 3.2 % (close to $\bar{v}_j^{*2}$); see Liu *et al.* (2014) for the mechanism behind the low non-dimensional velocity.

In addition to validating the velocity scaling in (1.1), both the Leidenfrost experiments and the numerical simulations also support the capillary–inertial time

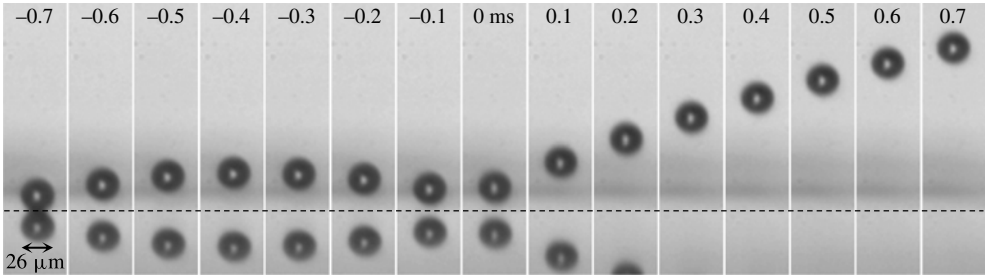

FIGURE 9. Spontaneous takeoff of an individual Leidenfrost drop with an initial radius of 13 μm. The vapour layer thickness fluctuates with an increasing magnitude (only the last cycle is shown), eventually leading to the spontaneous takeoff at 0 ms at a velocity of 0.22 m s^{-1}. The dashed line indicates the position of the Leidenfrost surface. See also supplementary movie 4.

scale in (2.1). For example, in both experimental figure 4 and numerical figure 6 the jumping departure occurs between 2.5 and 2.67 ms, consistent with the numerical observations in Liu *et al.* (2014) that the jumping process completes in $T_j \approx 0.8\pi\tau_{ci}$, which is 2.4 ms with $\bar{r}_0 = 380$ μm. After the departure, the half-period of oscillation is close to 1.5 ms ($\approx 0.5\pi\tau_{ci}$) in both experiments and simulations, e.g. from the oblate shape at 3.33 ms to the prolate shape at 4.83 ms.

For a drop radius below 30 μm or so, corresponding to $2r_{lub}$ in our experiments according to (1.2), the vapour layer thickness underneath a (quasi-)static Leidenfrost drop starts to fluctuate as a precursor to the breakdown of the lubrication regime. Such fluctuations are evident from the inset images of figure 8(*a*) showing visibly different vapour layer thicknesses with similar drop radii. For the open symbols in figure 8, the (average) drop–substrate gap at the initial coalescence is estimated to be between $0.1\bar{r}_0$ and $0.2\bar{r}_0$. A thicker vapour layer (i.e. a larger drop–substrate gap) leads to a smaller jumping velocity upon drop coalescence. The reduction in measured velocity is consistent with numerical simulations with the substrate relocated below the coalescing drops. The jumping velocities with vapour layer fluctuations are indeed bound by two numerical trend lines with a gap of $0.1r_0$ and $0.2r_0$, respectively (figure 8*b*). Note that the $\bar{v}_j \sim r_0^{-1/2}$ scaling is still observed with a gap between the coalescing drops and the substrate, of course with a smaller prefactor than is the case without a gap.

3.3. *Cutoff radius*

The numerical results in figure 8(*a*) indicate a cutoff radius around 0.1 μm due to viscous effects (Liu *et al.* 2014). The relative importance of viscous to capillary–inertial effects is characterized by the Ohnesorge number, $Oh = \mu_L/\sqrt{\rho_L \sigma r_0}$, where μ_L is the liquid viscosity. At the cutoff radius of $r_0 \approx 0.1$ μm, $Oh \approx 0.1$, so viscous effects become important and the jumping velocity deviates from the $\bar{v}_j \sim r_0^{-1/2}$ scaling law.

Unfortunately, the small viscous cutoff radius predicted by the numerical simulations cannot be accessed by our Leidenfrost set-up because of the spontaneous takeoff of individual drops (Celestini *et al.* 2012; Pomeau *et al.* 2012). The lower limit accessible by our Leidenfrost set-up is of the order of r_{lub} in (1.2), which is 15 μm for our experimental system. Below this limit, a single drop can spontaneously take off without any coalescence, as shown in figure 9 with a drop radius of 13 μm. After a few cycles of fluctuations, the slowly evaporating drop eventually takes off by itself.

Considering the possible fluctuations in the vapour layer thickness, the data taken around the lower radius bound should be interpreted with caution.

Although the Leidenfrost set-up cannot probe the numerically predicted cutoff radius of around 0.1 μm, it is important to emphasize that our experimental data on Leidenfrost surfaces are entirely consistent with the numerical model, as long as care is taken to exclude cases with strong fluctuations of the vapour layer (open symbols in figure 8). This consistency is a critical piece of evidence supporting the adequacy of our numerical model for the jumping-drop phenomenon. Given the agreement between Leidenfrost experiments and our numerical model assuming a flat non-wetting substrate, the cutoff radius of around 30 μm observed on superhydrophobic surfaces (Boreyko & Chen 2009) is probably due to the neglected interactions between the coalescing condensate drops and the textured superhydrophobic substrate; see Liu *et al.* (2014) for further discussions.

3.4. *Discussions*

Despite the agreement between Leidenfrost experiments and numerical simulations on the mass-averaged jumping velocities, the numerical model neglects some potentially important details of the experiments: (i) the presence of a vapour layer beneath Leidenfrost drops; (ii) the active evaporation of the Leidenfrost drops into the vapour layer; (iii) the dynamic approaching of drops ahead of coalescence; and (iv) the asymmetric coalescence between drops of unequal sizes and/or velocities. We shall now discuss why these details are not essential in the measurements of the jumping velocities. For the discussions here, we focus on cases with drop radii well above r_{lub}, where the lubricating vapour layer is thin (barely visible as in figure 4), and exclude cases where the vapour layer is appreciable compared to the drop radii (as in figure 8, bottom inset). The former cases with thin vapour layers are more typical of Leidenfrost surfaces and are the main focus of this experimental study.

The vapour layer plays a vital role in providing a non-wetting substrate simulated in Liu *et al.* (2014), but also introduces potential complications because the gaseous layer is compressible and the thin layer may entrain additional vapour from the evaporating drops. These complications are particularly relevant to the self-propelled jumping, which results from the reaction of the substrate to the impingement of the expanding liquid bridge. Based on our experimental results, which agree well with the simulations, the vapour layer appears to be acting primarily as a passive medium preventing the wetting of the substrate by the drops. Since the self-propelled jumping follows the capillary–inertial scaling with the local velocity within the merged drop (for which the mass-averaged value is $\bar{v}_j$) roughly bounded by u_{ci}, the impinging motion is naturally a low-Weber-number flow. Note that the Weber number here is still defined according to (2.4), although the impinging motion is perpendicular to the substrate while the approaching motion discussed in § 2.4 is parallel to the substrate. For perpendicular impingement with the corresponding Weber number less than unity, the vapour layer thickness should be much less affected compared to high-Weber-number impact (Tran *et al.* 2012), and the entrapment of air bubbles (Tran *et al.* 2013) has not been observed in the case of self-propelled jumping. In the related case of individual drops impinging on Leidenfrost surfaces, the low-Weber-number impact is known to be quasi-elastic with a nearly perfect rebound (Biance *et al.* 2006), unlike the much more dissipative impact at high Weber numbers (Clanet *et al.* 2004).

The vapour layer is constantly replenished by the evaporation of the Leidenfrost drops, and the active evaporation may explain the observation in figure 8 that the

measured jumping velocities are slightly higher than the numerical ones (when $\bar{r}_0 \gg r_{lub}$). For a quasi-static drop, the vapour layer thickness varies over radial position (Snoeijer *et al.* 2009; Burton *et al.* 2012) but can be assumed invariant over time periods shorter than the life span of the Leidenfrost drop (Quéré 2013). For the rapid jumping process induced by coalescence, additional vapour may be entrained as the vapour layer is mildly compressed during the impingement of the liquid bridge. A slightly higher evaporation rate presumably results in an augmented rebound velocity in figure 8. An analogous observation (and explanation) is reported in Biance *et al.* (2006), where the rebound velocity from a Leidenfrost surface is higher than the impacting velocity of an individual drop. Note that the augmentation in jumping velocities cannot be attributed to the compression of a completely passive gas layer alone, in which case the compression will lead to energy dissipation and subsequent reduction in the rebound velocity.

The coalescence in the experiments is usually between drops with a net approaching velocity, unlike the coalescence of initially static drops in the simulations. In figure 5, the approaching velocity can be a few times larger in magnitude than the ultimate jumping velocity, yet the measured jumping velocity agrees very well with the simulated case without any approaching velocity. The agreement suggests that the approaching velocity is not important in the experimentally tested regime of low-Weber-number coalescence with $v_{app} < u_{ci}$. This conclusion is in line with the observation in our companion paper that purely oscillatory motion can be artificially turned off at any instant (e.g. the point of coalescence) without significantly affecting the resulting translational jumping velocity (Liu *et al.* 2014, § 4.3.2). The symmetric collision is analogous to a purely oscillatory motion that is inconsequential to the eventual jumping velocity.

In our experiments, the coalescence between two drops is always somewhat asymmetric. The asymmetry can arise from the disparity in approaching velocities or drop radii. The asymmetry in approaching velocities may be translational in the horizontal direction (discussed in the preceding paragraph), vertical along the jumping direction, or rotational. The difference in drop shapes between figures 4 and 6 can be partially attributed to asymmetric approaching velocities. For example, we have noticed that most approaching drops have a slight bouncing motion as well as a self-rotation, which might lead to the dimple at 2.17 ms in figure 4. For drop radii that are close, the average radius is sufficient for the numerical simulations. For example, simulation using initially static drops with radii of 370 and 390 μm to match figure 4 yields a jumping velocity nearly identical (within 1 %) to the simulation in figure 6 assuming an equal radius of 380 μm. For drop radii that are significantly different, the jumping process is much more complicated (figure 10) as discussed in appendix A.

4. Conclusions

Using Leidenfrost surfaces, we have studied the coalescence-induced jumping motion that is originally reported on superhydrophobic surfaces. The key advantage of the Leidenfrost set-up is the intercalating vapour layer between the coalescing drops and the heated substrate, giving rise to a simpler boundary condition that is closer to the numerical assumption of a flat surface with a contact angle of 180° (Liu *et al.* 2014). On the other hand, the Leidenfrost set-up also introduces new challenges, particularly for small drops with potentially fluctuating vapour layer thickness.

The Leidenfrost experiments have quantitatively confirmed the numerically predicted jumping velocities for initial drop radii between 20 and 500 μm. For

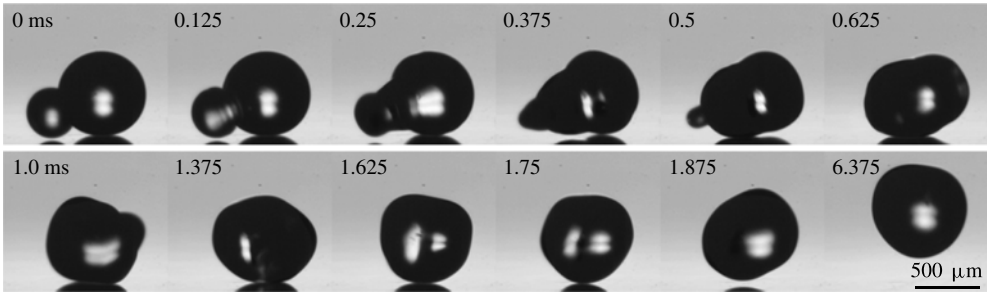

FIGURE 10. Asymmetric coalescence between drops with a radius of 330 μm and 190 μm, respectively. The smaller drop approaches from behind the larger quasi-static drop at a velocity of 0.02 m s^{-1}, giving rise to a negligible horizontal velocity of around 0.004 m s^{-1} for the merged drop. The jumping velocity in the vertical direction is 0.05 m s^{-1}. See also supplementary movie 5.

this experimentally accessible range of radii, the capillary–inertial velocity scaling is followed and no cutoff radius is observed. The Leidenfrost experiments support the adequacy of our numerical model in Liu *et al.* (2014) as a first step in uncovering the physical mechanism of the self-propelled jumping motion. To fully model the jumping motion on superhydrophobic surfaces, a more faithful boundary condition will be a logical next step.

Acknowledgements

F.L. and C.-H.C. were supported by the National Science Foundation (CBET-08-46705 and CBET-12-36373) and the Defense Advanced Research Projects Agency (N66001-10-1-4048). G.G. and J.J.F. were supported by the Canada Research Chair program, Natural Sciences and Engineering Research Council (Discovery and Strategic grants and Accelerator Supplement), and the Canada Foundation for Innovation. The authors acknowledge J. Boreyko for his work at the initial phase of the project.

Supplementary movies

Supplementary movies are available at http://dx.doi.org/10.1017/jfm.2014.319.

Appendix A. Asymmetric coalescence

Asymmetric coalescence is difficult to study with the set-up in figure 2 because of the residual horizontal momentum. To circumvent this difficulty, a bowl-shaped Leidenfrost surface with a slight curvature is used to trap a larger drop in the centre with minimal horizontal momentum, and then a smaller drop is created nearby through boiling with a combination of the exploding and gating methods (similar to those in § 2.2). Gravity drives the smaller drop towards the centre to coalesce with the larger quasi-static one (figure 10). Other experimental conditions are kept the same as the main set-up.

Compared to the symmetric coalescence, the asymmetric coalescence and the ensuing drop–substrate interaction represented by figure 10 are much more complex. The expanding liquid bridge impinges upon the substrate obliquely instead of perpendicularly, and the horizontal oscillation of the merged drop complicates the

interaction with the substrate. Capillary waves triggered by the coalescence process, initially travelling away from the substrate, are eventually bounced back towards the substrate. The reflected waves add to the impingement process due to the expanding liquid bridge, the latter being the only mode of impingement in the symmetric case. In addition, satellite drops can be generated (and subsequently absorbed) in some cases, as shown in figure 10. Such satellite drops are not observed in the (nearly) symmetric coalescence case in our experimental regime of low Weber number. These observations are analogous to satellite formation during asymmetric coalescence in the absence of a substrate (Zhang, Li & Thoroddsen 2009).

For asymmetric coalescence with the radius of one drop (r_1) significantly smaller than the other (r_0), the released surface energy scales with the surface area of the smaller drop (σr_1^2), while the merged mass is dominated by the larger drop, so its kinetic energy scales as $\rho_L r_0^3 \bar{v}_{j,a}^2$. From an energetic argument similar to (1.1), the jumping velocity ($\bar{v}_{j,a}$) for asymmetric coalescence with $r_1 \ll r_0$ scales as

$$\bar{v}_{j,a} \sim \frac{r_1}{r_0} u_{ci} = \frac{r_1}{r_0} \sqrt{\frac{\sigma}{\rho_L r_0}}. \tag{A 1}$$

Alternatively, this scaling relation can be recovered as a limit of equation (2) in Boreyko & Chen (2009). According to (A 1), the jumping velocity for the asymmetric coalescence is expected to reduce by a factor of r_1/r_0 compared to the symmetric coalescence with an initial radius of r_0. With $r_0 = 330$ μm and $r_1 = 190$ μm, the measured asymmetric jumping velocity is 0.05 m s^{-1} (figure 10), while the corresponding symmetric jumping velocity is 0.08 m s^{-1} (figure 5). The ratio of the asymmetric and symmetric jumping velocity is 0.6, which is close to $r_1/r_0 = 0.58$. Although the quantitative agreement with the scaling equation (A 1) is somewhat coincidental, our experimental results do support the reduction in non-dimensional jumping velocity for asymmetric coalescence; more measurements can be found in Liu (2013). Given the complexity of asymmetric coalescence, a more systematic study is required for future work.

REFERENCES

Bernardin, J. D. & Mudawar, I. 1999 The Leidenfrost point: experimental study and assessment of existing models. *Trans. ASME: J. Heat Transfer* **121**, 894–903.

Biance, A. L., Chevy, F., Clanet, C., Lagubeau, G. & Quéré, D. 2006 On the elasticity of an inertial liquid shock. *J. Fluid Mech.* **554**, 47–66.

Biance, A. L., Clanet, C. & Quéré, D. 2003 Leidenfrost drops. *Phys. Fluids* **15**, 1632–1637.

Boreyko, J. B. 2012 From dynamical superhydrophobicity to thermal diodes. PhD thesis, Duke University, Durham, NC.

Boreyko, J. B. & Chen, C. H. 2009 Self-propelled dropwise condensate on superhydrophobic surfaces. *Phys. Rev. Lett.* **103**, 184501.

Boreyko, J. B. & Chen, C. H. 2010 Self-propelled jumping drops on superhydrophobic surfaces. *Phys. Fluids* **22**, 091110.

Burton, J. C., Sharpe, A. L., van der Veen, R. C. A., Franco, A. & Nagel, S. R. 2012 Geometry of the vapor layer under a Leidenfrost drop. *Phys. Rev. Lett.* **109**, 074301.

Celestini, F., Frisch, T. & Pomeau, Y. 2012 Take off of small Leidenfrost droplets. *Phys. Rev. Lett.* **109**, 034501.

Clanet, C., Béguin, C., Richard, D. & Quéré, D. 2004 Maximal deformation of an impacting drop. *J. Fluid Mech.* **517**, 199–208.

GOTTFRIED, B. S., LEE, C. J. & BELL, K. J. 1966 The Leidenfrost phenomenon: film boiling of liquid droplets on a flat plate. *Intl J. Heat Mass Transfer* **9**, 1167–1188.

LEIDENFROST, J. G. 1756 *De Aquae Communis Nonnullis Qualitatibus Tractatus*. Johann Straube, Duisburg (translation: 1966 *Intl J. Heat Mass Transfer* **9**, 1153–1166).

LIU, F. 2013 Self-propelled jumping upon coalescence on Leidenfrost surfaces. MS thesis, Duke University, Durham, NC.

LIU, F., GHIGLIOTTI, G., FENG, J. J. & CHEN, C.-H. 2014 Numerical simulations of self-propelled jumping upon drop coalescence on non-wetting surfaces. *J. Fluid Mech.* **752**, 39–65.

NEITZEL, G. P. & DELL'AVERSANA, P. 2002 Noncoalescence and nonwetting behavior of liquids. *Annu. Rev. Fluid Mech.* **34**, 267–289.

POMEAU, Y., LE BERRE, M., CELESTINI, F. & FRISCH, T. 2012 The Leidenfrost effect: from quasi-spherical droplets to puddles. *C. R. Méc.* **340**, 867–881.

QIAN, J. & LAW, C. K. 1997 Regimes of coalescence and separation in droplet collision. *J. Fluid Mech.* **331**, 59–80.

QUÉRÉ, D. 2005 Non-sticking drops. *Rep. Prog. Phys.* **68**, 2495–2532.

QUÉRÉ, D. 2013 Leidenfrost dynamics. *Annu. Rev. Fluid Mech.* **45**, 197–215.

SNOEIJER, J. H., BRUNET, P. & EGGERS, J. 2009 Maximum size of drops levitated by an air cushion. *Phys. Rev.* E **79**, 036307.

TRAN, T., DE MALEPRADE, H., SUN, C. & LOHSE, D. 2013 Air entrainment during impact of droplets on liquid surfaces. *J. Fluid Mech.* **726**, R3.

TRAN, T., STAAT, H. J. J., PROSPERETTI, A., SUN, C. & LOHSE, D. 2012 Drop impact on superheated surfaces. *Phys. Rev. Lett.* **108**, 036101.

ZHANG, F. H., LI, E. Q. & THORODDSEN, S. T. 2009 Satellite formation during coalescence of unequal size drops. *Phys. Rev. Lett.* **102**, 104502.